Experimental methods for visualization of hydrodynamic instability caused by the neutralization reaction in a miscible two-layer system

Elena Mosheva

Institute of Continuous Media Mechanics of the Ural Branch of the Russian Academy of Sciences, 614000, Perm, Russia

Abstract. This paper focuses on experimental investigations of the spatio-temporal distributions of fluid velocity and temperature and the concentration of reagents and reaction products. We study concentration-dependent diffusion (CDD) convection driven by the neutralization reaction in a two-layer miscible system in a vertical Hele-Shaw cell using the original experimental complex. A comprehensive understanding of the physical mechanisms of convective motion and instabilities requires employing various experimental methods simultaneously. The proposed experimental complex provides simultaneous visualization and facilitates identification of the location of the reaction front, which is of importance to the study of its characteristics.

1 Introduction

Investigation of the chemo-hydrodynamic patterns is necessary for studying heat and mass transfer processes, hydrodynamic instability mechanisms and convective flow structure and its evolution in a two-layer system of reacting fluids. Composition and temperature changes accompanying chemical reactions have a strong impact on the examined system. In particular, non-isothermicity and continuous changes in the concentrations of reagents and reaction products may lead to changes in density, viscosity and diffusion rate. These variations of the fluid properties may result in the formation of buoyancy-driven instabilities [1, 2].

On the basis of the study of the asymptotics of large evolution times of the system, a general classification of all possible types of instabilities was proposed in [3]. Double-diffusion (DD convection), diffusive-layer (DLC convection), and Rayleigh–Taylor (RT convection) instabilities were revealed. However, due to the fact that the diffusion coefficients of reagents depend on the concentration of solutions, the density profile may drastically change in time, which was not taken into account in the proposed classification. It was shown both experimentally and theoretically that concentration-dependent diffusion coupled with frontal acid-base neutralization reaction can produce a spatially localized zone with unstable density stratification which, under gravity, gives rise to the onset of the instability called concentration-dependent diffusion convection (CDD convection) [4].

There are a lot of experimental methods for studying the characteristics of such reactive liquid systems and instabilities. High-precision optical methods, which are based, for example, on interferometry [5] or shadowgraph technique [6], are employed to visualize a refractive index distribution caused by the temperature and concentration inhomogeneities. To visualize a convective flow structure and pattern formation process, the tracer particles method is used. The addition of chemical indicators allows visualizing the pH distribution, which makes it possible to identify reagents and reaction products in space. Temperature changes due to the exothermic (endothermic) nature of the reaction are investigated by thermocouple methods [7].

All these methods are usually employed separately from each other. Such an approach hinders true understanding of the physical mechanisms responsible for the occurrence of convective motion and instabilities. Thus, a comprehensive study of the problem requires employing various techniques simultaneously.

In this paper, we present an experimental complex to simultaneously visualize and study the spatio-temporal distribution of fluid velocity and temperature, as well as the concentration of reagents and reaction products. The proposed complex was tested by investigating CDD convection driven by the frontal neutralization reaction in a two-layer miscible system in a vertically oriented Hele-Shaw cell.

2 Experimental setup

The experiments were performed in a vertically oriented Hele-Shaw cell with dimensions $9.0\times2.4\times0.12$ cm^3. Aqueous solutions of nitric acid HNO_3 and sodium hydroxide NaOH with molar concentration $C_a = 1$ mol/l and $C_b = 1$ mol/l, respectively, were used as reagents. Such concentrations were chosen according to the map of the reaction regimes for the HNO_3/NaOH system presented in [5], in which these concentrations are in the

* Corresponding author: mosheva@icmm.ru

range within which CDD convection arises. Reagents were separated by a thin plastic shutter before they come into contact. This allows one to avoid an untimely onset of the reaction and to provide the initially flat horizontal interface between the layers. The lower layer was first filled with a denser base solution and then tightly covered by a shutter. The upper layer was filled with an equimolar solution of a less dense acid. After that, the shutter was carefully taken out of the cell, the reactants were brought into contact, and the reaction started. All experiments were performed at room temperature (24±1) °C.

2.1 Interferometer

The experimental setup was developed using the concept of the Fizeau interferometer with an autocollimation circuit assembled as shown in figure 1. The light beam of constant frequency He-Ne laser 1 (wavelength $\lambda = 633$ nm) is expanded by lens 2 and passes through collimator 4. The formed parallel laser beam of large diameter falls on the lateral face of the cell with reacting system 5 under study. Part of the light beam reflected from the front cell wall is the reference beam. Another part of the light is transferred through the reacting system and reflects from the rear (in the direction of the beam) cell wall, forming the object beam. Finally, the reflected fringe patterns are captured by CCD camera 6.

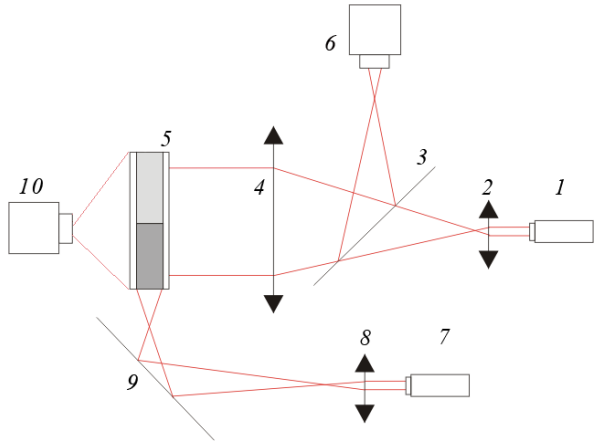

Fig. 1. Sketch of the experimental setup.

A change in the refractive index occurs in the system due to the variation of density, which is a function of a set of variables:

$$\rho = \rho(T, C_a, C_b, C_s), \qquad (1)$$

where ρ is density, T is temperature, C_a, C_b, C_s are the molar concentrations of the aqueous solutions of the acid, base, and salt, respectively. Thus, contributions to the variation of the total density are of two sorts: concentration (due to the change in the concentrations of reagents and the reaction product) and thermal (due to the exothermic nature of the neutralization reaction). The maximum temperature increase measured in the vicinity of the reaction front was found to be near $\Delta T = 1$ K. In this case, the refractive index deviation due to temperature was at least one order of magnitude smaller than that caused by concentration. Thus, the interferograms obtained in the experiments reflected mainly the density variations caused by the change in the concentrations of the reactants and the reaction product.

However, quantitative data on the concentration distribution separately for each substance cannot be obtained by the proposed method. In the system under investigation, the mutual diffusion of acid and base is a priori impossible, since they are initially separated by the reaction zone, which prevents their penetration. The mutual diffusion process takes place only between salt and reagents. In the upper layer, diffusion occurs between the salt and the acid and, in the bottom layer, between the salt and the base. Thus, there are always three components in each layer, namely water, one of the reagents and salt. The problem of getting the concentration (density) profile in a ternary mixture is quite common and, as shown by the literature search [8-10], is successfully solved using the double-reflecting interferometry technique. However, the purpose for use of an interferometer in our investigation is to obtain qualitative rather than qualitative information about the concentration distribution. Furthermore, due to the large Schmidt numbers *Sc* typical of the reactive system, one can investigate the structure of convective flow using a single-beam interferometer. The value of *Sc* is expressed as

$$Sc = \frac{\tau_D}{\tau_v} = \frac{L^2}{D}\frac{\nu}{L^2} = \frac{\nu}{D} = \frac{10^{-2}}{10^{-5}} = 10^3, \qquad (2)$$

where τ_D, τ_v are the diffusive and viscous times, respectively, ν is the kinematic viscosity, and D is the diffusion coefficient. At high Schmidt numbers, the concentration isolines are 'frozen' in the moving media and the use Fizeau interferometer makes it possible to determine the structure of flows and to investigate its evolution in real time.

2.2 Tracer particles

The convective patterns formed during the reaction were also visualized by the tracer particles method. The particles were silver-coated hollow glass spheres with an average diameter of 20 μm, which were added to the solutions during their preparation. A relative volume concentration of the particles in the solution did not exceed 10^{-3}%. Due to the fact that the density of particles varied over a wide range, the fraction with neutral buoyancy was selected during the separation process. The particles were placed in a vessel with water for one hour (the reference time span of the experiment). In the course of time, the particles were distributed throughout the layer depth. Under gravity, the heavy fraction settled to the bottom, and the light fraction rose to the surface. The fraction with neutral buoyancy was taken from the middle part of the layer by a syringe. The use of a fraction with neutral buoyancy made it possible to achieve the uniform distribution of tracers in the experimental cell and to avoid the buoyancy-driven particle motions. The laser sheet was produced by laser 7 and lens 8. Using mirror 9, the laser sheet was directed

through the transparent bottom of the cell. Passing along the middle plane of the cell, the sheet illuminated the light-scattering particles. A video recording of the particles' motion was carried out by camera 6.

2.3 pH indicator

In order to visualize the spatial distribution of the reagents and the reaction product, the universal indicator was used. The universal indicator is a combination of several indicators (thymol blue, methyl orange, bromothymol blue, phenolphthalein, tropaeolin OO, bromocresol green and bromocresol purple), that display colors at pH values inside the certain transition range. That is why the universal indicator displays color changes over a wide pH value range from 1 to 10. Colors from orange to red indicate an acidic solution, colors from light to dark blue indicate bases, and colors from yellow to green indicate that the solution is neutral. The use of the color indicator has a significant advantage against the background of another visualization tools. It facilitates to see where the reaction front is, which is essential for studying its properties.

The indicator was prepared on the basis of the aqueous solution of ethanol with mass concentration $w = 80\%$. The initial concentration and density of the indicator were 2×10^{-4} mol/l and 0.849 g/cm^3, respectively. The indicator was added to the reagent solutions before the start of the experiment. In order to obtain a visualization of the pH distribution, the light beams from the lasers 1 and 7 blocked up with a sheet of white paper that was placed between the cell 5 and the collimator 4. Then the spatial distribution of the reagents was observed by camera 10.

Because of the fact that physical parameters (viscosity, density, diffusivity) of the reagents and the indicator are different, the use of latter may result in the appearance of additional driving forces of convection and even give rise to the pattern formation in the system. In some research [11-13] it was shown both experimentally and numerically that the presence of an indicator in the system leads to the formation of hydrodynamic instabilities that are not observed in their absence. In this context, the influence of the universal indicator on the stability of a miscible two-layer reactive system has been previously studied [14]. It was found out that the indicator with relative volume concentrations not exceeding 0.2% does not affect the system stability. While such indicator concentrations are negligible for the system mechanics, they are sufficient to have a good visualization. The influence of the universal indicator on the stability of a two-layer system is discussed in [14] in detail.

2.4 Thermocouples

The temperature changes ΔT due to reaction exothermicity was measured by a copper-constantan thermocouple with one contact point mounted inside the reacting system and the other (for the reference temperature) located in the thermostat at a fixed temperature. The diameter of the used wire is $d = 0.014$ cm. The thermocouples' wires were located tube with an external diameter $d = 0.07$ cm from the inside. The tube was filled with a chemically resistant sealant, which served as a heat insulator. The thermocouple contact point was outside the tube. The tube with a thermocouple was attached to a special device so that the vertical coordinate of the thermocouple contact point could be changed with an accuracy of 0.01 cm. The output signal obtained from the thermocouple was determined with an analog-to-digital converter from the National Instruments. Either the voltage signal or the indicated temperature for each test was recorded with frequency 5 Hz. The accuracy of the obtained results was controlled by repeated experiments and measurements.

3 Results

When the prepared solutions come into contact, a diffusion zone appears between them. At the same time, the occurrence of DLC instability above the diffusion zone gives rise to the formation of plumes which results in the development of weak buoyancy-driven convection in the upper layer, while the area below the diffusion zone remains motionless (a detailed explanation of the DLC formation mechanism is given in [4]). Some time later, CDD convection in the form of a horizontal array of convective cells arises within the diffusion zone.

The CDD convection patterns visualized using the above described experimental complex are given in figure 2. Each row demonstrates the evolution of the density field (Fig. 1 a, d, g), the flow structure (Fig. 1 b, e, h) and the pH distribution (Fig. 1 c, f, i) obtained simultaneously. The first row represents the initial stage of the CDD instability formation (300 seconds after the reagents come into contact). The interference image demonstrates (Fig. 1 a) that the diffusion zone is initially stably stratified as indicated by horizontal interference fringes. Convective motion is only in the upper layer, which is clearly seen in the flow structure image (Fig. 1 b). Observations of the pH distribution (Fig. 1 c) allow identifying the reaction front. Since the concentration of salt at the front is maximum, it is visualized as a thin localized zone with acidity close to neutral (bright in grayscale), which clearly indicates product (salt) accumulation.

Simultaneous visualization of the density and acidity field makes it possible to identify the location of the reaction front. Based on the comparison of images with density and pH distribution, it can be concluded that the reaction front is localized inside the diffusion zone. This is also evidenced by the distribution of the temperature measured along the vertical direction, which indicates the maximum heat output at the lower boundary of cells. In each row on the Fig. 1, the reaction front is indicated by the dashed line.

Analysis of the interference image (Fig. 2 a) has revealed that the cellular structure does not interact with convection in the upper layer. The cells are confined between two thin layers of the immobile fluid. Horizontal fringes inside these layers definitely indicate the presence of stable stratification within them and the

formation of a local 'pocket' with unstable density stratification between them, which causes a cellular pattern to occur (Fig. 2 b). Observations of the pH distribution (Fig. 2 c) show that above and below the cell zone the medium has almost homogeneous pH (acidic or alkaline). The pH within the cellular structure is more neutral, indicating the accumulation of the reaction product in this region. The pH images demonstrate the fine structure of the cell interior. The downstreams of the cells are red (dark in grayscale), indicating that the acid is entrained by the flow. The upstreams are enriched with salt (bright in grayscale), which points out that the reaction occurs at the lower edge of the cellular structure.

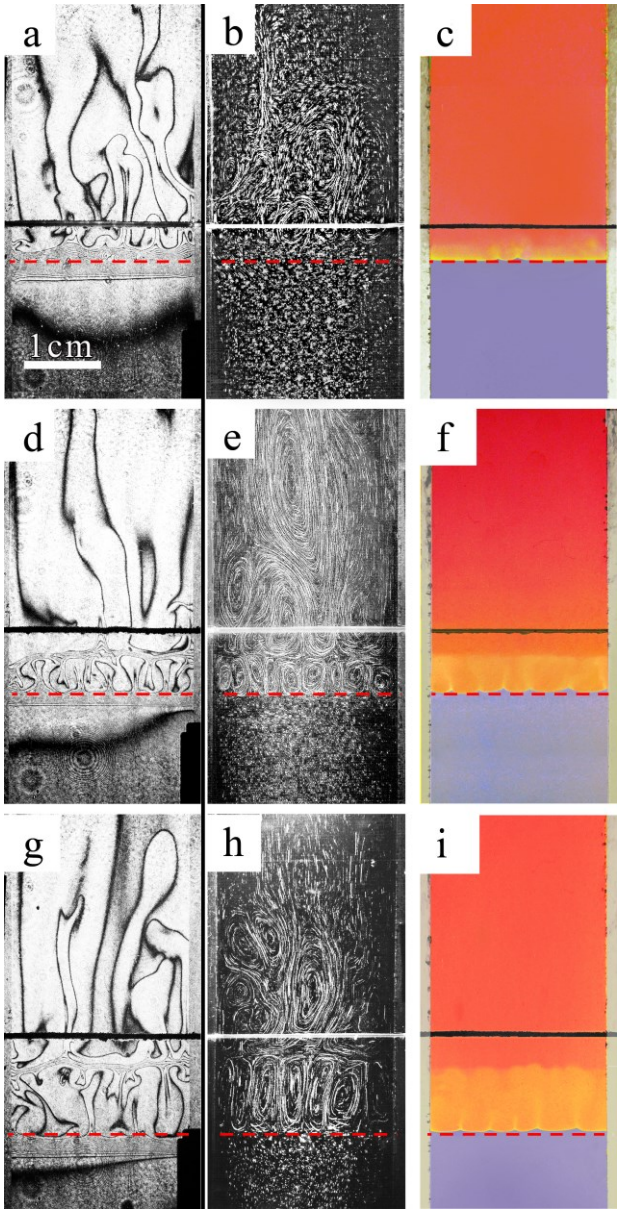

Fig. 2. Density field, flow structure and pH distribution obtained at deferent times after the experiment started. First row (a, b, c) - 300 s; second row (d, e, f)- 1100 s; third row (g, h, I) - 2250 s. The black horizontal line is the initial contact line.

4 Conclusions

The experimental complex developed for visualization of the pattern formation driven by acid-base reactions in the vertical Hele-Shaw enabled employing several experimental methods simultaneously. In particular, the Fizeau interferometer-based technique was used to study concentration fields, and the tracer particles method - to visualize the flow structure. Temperature measurements and visualization with the aid of the color indicator made it possible to identify the reaction front location and to visualize the spatial distribution of reagents and products. The simultaneous application of several experimental methods provides a comprehensive study of the properties of the system itself and the processes taking place in it.

The author wants to thank A. I. Mizev for fruitful discussions. Appreciation also goes to A. V. Shmyrov for help with experiments. The reported study was supported by RFBR, research project No. 18-31-00308 mol_a.

References

1. C. Almarcha, P. M. J. Trevelyan, P. Grosfils, A. de Wit, Phys. Rev. Lett , **104**, 044501 (2010)
2. A. Zalts, C. El Hasi, D. Rubio, A. Urena, A. D'Onofrio, Phys. Rev. E, **77**, 015304 (2008)
3. P. M. J. Trevelyan, C. Almarcha, A. de Wit, Phys. Rev. E, **91**, 023001 (2015).
4. D. Bratsun, K. Kostarev, A. Mizev, and E. Mosheva, Phys. Rev. E **92**, 011003 (2015)
5. D. Bratsun, K. Kostarev, A. Mizev, and E. Mosheva, Phys. Rev. E **96**, 053106 (2017)
6. P. Bunton, D. Marin, S. Stewart, E. Meiburg, A. De Wit, Experiments in Fluids **57**, 28 (2016)
7. K. Eckert, M. Acker, Y. Shi, Phys. of Fluids, **16**, 385(2004)
8. A. Königer, H. Wunderlich, W. Köhler, J. Chem. P. **132**, 174506 (2010).
9. V. Sechenyh, J. C. Legros, V. Shevtsova, J. Chem. Eng. Data **57**, 1036 (2012)
10. O. A. Khlybov, I. I. Ryzhkov, T. P. Lyubimova, Eur. Phys. J. E **38**, 29 (2015)
11. C. Almarcha, P. M. J. Trevelyan, L. A. Riolfo, A. Zalts, C. El Hasi, A. D'Onofrio, A. De Wit J. Phys. Chem. Lett. **1**, 752 (2010)
12. S. Kuster, L. A. Riolfo, A. Zalts, C. El Hasi, C. Almarcha, P. M. J. Trevelyan, A. De Wit , A. D'Onofrio Phys. Chem. Chem. Phys. **13**, 17295 (2011)
13. T. Nisimura, K. Tanoue, T. Watanabe, Y. Itoh, K. Kunitsugu Trans. Japan Soc. Mech. Eng. **72**, 1773 (2006)
14. E. A. Mosheva, A. V. Shmyrov, IOP Conference Series: Materials Science and Engineering **208**, 012029 (2017)